Ionization of molecular hydrogen and deuterium by a frequency-doubled Ti:sapphire laser pulses

Yulian V. Vanne and Alejandro Saenz
AG Moderne Optik, Institut für Physik, Humboldt-Universität zu Berlin, Hausvogteiplatz 5-7, D – 10 117 Berlin, Germany
(Dated: September 18, 2009)

A theoretical study of the intense-field single ionization of molecular hydrogen or deuterium oriented either parallel or perpendicular to a linear polarized laser pulse (400 nm) is performed for different internuclear separations and pulse lengths in an intensity range of $(2-13)\times10^{13}\,\mathrm{W\,cm^{-2}}$. The investigation is based on a non-perturbative treatment that solves the full time-dependent Schrödinger equation of both correlated electrons within the fixed-nuclei and the dipole approximation. The results for various internuclear separations are used to obtain the ionization yields of molecular hydrogen and deuterium in their ground vibrational states. An atomic model is used to identify the influence of the intrinsic diatomic two-center character of the problem.

PACS numbers: 32.80.Rm, 33.80.Rv

I. INTRODUCTION

The theoretical and experimental investigation of the interaction of molecules with intense laser fields remains one of the most challenging problems of atomic, molecular, and optical physics. Despite the numerous experimental work on molecules in intense ultrashort laser pulses during the last decades (see, e. g., [1, 2] for reviews) a full understanding of the influence of the molecular structure on the strong-field response is still lacking. However, such an understanding is a prerequisite for the recently proposed techniques that aim for the time-resolved imaging of changes of the electronic structure during chemical reactions. The development of such imaging techniques is driven by successful pioneering experiments in which the strong-field induced high-harmonic radiation [3] or the in the ionization process ejected electrons [4] were used to image the highest-occupied molecular orbitals of molecular nitrogen or oxygen.

In order to achieve a three-dimensional image of the electron density or even an electronic orbital it is of course important to perform a spatially resolved measurement. Often, field-free alignment by means of rotational wave-packets [5, 6] is adopted for providing angle-resolved molecular strong-field data [4, 7, 8, 9], but in [10, 11] alternative techniques without alignment are used. These experimental efforts are accompanied by a number of theoretical investigations of the orientational dependent ionization probability of molecules in intense laser pulses. Since most molecular systems require some approximative treatment like the strong-field approximation based additionally on the single-active electron approximation (SAE) [12, 13, 14, 15] or an effective independent-particle model like the time-dependent density-functional theory (TD-DFT) [16], the simplest neutral stable molecule, H_2 whose orientational dependence [10, 11, 17] or angular distribution of ejected electrons [18] was recently investigated experimentally is, in principle, an attractive alternative. Solutions of the time-dependent Schrödinger equation (TDSE) describing both electrons of H_2 exposed to an intense laser pulse in full dimensionality became recently available [19, 20, 21]. However, these calculations were restricted to a parallel orientation of the molecule with respect to the field axis of a linear-polarized laser. This simplifies the treatment drastically, since the problem reduces to five spatial dimensions, as the cylindrical symmetry is preserved.

Theoretical investigations of the orientational dependence of the strong-field behavior of H_2 are thus rather limited so far. This includes studies within the lowest-order perturbation theory (LOPT) [22], TD-DFT [23], or a Hartree-Fock based SAE approach [24]. The validity of the SAE (and simplified models like the molecular Ammosov-Delone-Krainov tunneling model (MO-ADK) or the molecular strong-field approximation (MO-SFA)) that reduces the problem to three spatial dimensions was investigated in [25] and found to be problematic especially for few-photon processes. Only very recently the first investigation of the orientational dependence of the behavior of H_2 in ultrashort intense laser pulses based on the TDSE was presented [26], and thus a full treatment of all six spatial dimensions of the two electrons was achieved. In [26] the single-ionization yield for a parallel and a perpendicular orientation was compared as a function of the wavelength, spanning an interval between about 50 and 400 nm. Considering two different laser intensities and nuclear distances, only a brief idea of the influence of these parameters was provided.

In the context of imaging it is, however, important to investigate in which way laser intensity or the quantum-mechanically unavoidable zero-point vibrational motion may blur the obtained image. On the other hand, the strong-field response itself may be used to visualize nuclear dynamics with sub-femtosecond resolution [27, 28, 29, 30, 31, 32, 33]. In fact, for molecules like H_2 a strong influence of nuclear motion on the strong-field ionization behavior was predicted on the basis of a simple model in [34] and later confirmed by *ab initio* calculations of quasistatic rates [35, 36, 37, 38] and full TDSE calculations [39]. An experimental confirmation for 800 nm radiation was achieved by the observation of

strong deviations from the Franck-Condon distribution of the formed H_2^+ vibrational states [40] and the occurrence of vibrational wavepackets in neutral H_2 due to a phenomenon called *Lochfraß* [31] that had been theoretically predicted in [30]. However, the responsible strong dependence of the ionization yield on the internuclear distance was predicted for the so-called quasi-static regime, i. e. for low frequencies (long wavelengths) and high intensities. On the other hand, the perturbative results in [22] indicated that the dependence on the internuclear distance is expected to be rather small in this so-called multiphoton regime (high frequency and low intensity).

This work investigates the intensity and internuclear-distance dependence of the single-ionization yield of parallel or perpendicular aligned H_2 in ultrashort linear-polarized laser pulses with a wavelength of about 400 nm, as they are, e. g., experimentally available from a frequency doubling (second-harmonic generation) of a titanium-sapphire laser source. Besides the experimental relevance, the chosen wavelength is also of theoretical interest, since one expects six-photon ionization processes to dominate which lie somehow in the middle between few-photon and many-photon regimes. Thus one expects neither a simple perturbative nor the quasistatic approximation to be applicable. This ambivalent character is shown to be clearly visible, since, e. g., the ionization yield shows a pronounced dependence on the internuclear separation (as is expected for the quasistatic regime), but also clear structures due to resonance-enhanced multiphoton ionization (REMPI). However, these structures are to a large extent washed out, if one goes beyond the fixed-nuclei approximation. In the present work vibrational motion is considered in an approximate way where the internuclear-separation dependent ionization yields are weighted by the vibrational wavepacket of the initial state. The resulting ionization yields of H_2 and D_2 are compared with each other to resolve the isotope effect. Since for very short laser pulses the pulse duration influences the strong-field behavior, the effects of the laser-pulse duration are investigated considering pulse lengths of 5, 10, and 20 fs. In the following atomic units ($e = m_e = \hbar = 1$) are used unless specified otherwise.

II. METHOD

Our method of solving the TDSE describing molecular hydrogen exposed to a laser field for parallel orientation and its extension to the perpendicular one is discussed in detail in [20] and [26], respectively. Briefly, the TDSE is solved by expanding the time-dependent wave function in terms of field-free states. The latter are obtained from a configuration-interaction (CI) calculation [41] in which the Slater determinants are formed with the aid of H_2^+ wave functions expressed in terms of B splines in prolate spheroidal coordinates ($1 \leq \xi < \infty, -1 \leq \eta \leq 1, 0 \leq \phi < 2\pi$). The use of a B-spline basis confined within a finite spatial volume defined by parameter $\xi_{\max}$ results in a suitable discretization of the electronic continuum.

A. Configuration-interaction calculation

For the considered laser parameters the electronic field-free states for every molecular symmetry were obtained as follows. A box size of about $350\,a_0$ is chosen independently of R. This is achieved by a proper adaption of $\xi_{\max}$ as a function of R. Along the ξ coordinate 350 B splines of order $k = 10$ with an almost linear knot sequence were used where the first 40 intervals are increased by a geometric progression using a progression factor $g = 1.05$ and then the size of the interval remains constant. Along the η coordinate 30 B splines of order 8 were used in the complete interval $-1 \leq \eta \leq 1$, but using the symmetry of a homonuclear system as is described in [41]. Out of the resulting 5235 orbitals for every symmetry only 3490 orbitals were further used to construct CI configurations, whereas those orbitals with highly oscillating angular part (with more than 19 nodes for the η-dependent component) were omitted. In most of the subsequent CI calculations approximately 6000 configurations were used for every symmetry. These states result from a very long configuration series (3490 configurations) in which one electron occupies the H_2^+ ground-state $1\,\sigma_g$ orbital while the other one is occupying one of the remaining, e. g., $n\,\pi_u$ or $n\,\delta_g$ orbitals. The other CI configurations represent doubly excited situations and are responsible for describing correlation (and real doubly excited states). Finally, out of the obtained CI states only those with an energy below the energy cut-off (chosen at 10 a.u. above the ionization threshold for the calculations shown in this work) were included in the time propagation (about 5400 states per symmetry). For the perpendicular orientation only molecular symmetries with the absolute value of the component of the total angular momentum along the internuclear axis $0 \leq \Lambda \leq 7$ were included in the time propagation. This results in a system of about 86,000 real-valued first-order differential equations. Noteworthy, the adopted range of Λ values does not only guarantee the convergence of ionization yields, but also provides a reasonable description of photoelectron energy spectra.

The basis set specified above was chosen to provide a good compromise for describing a large number of states and can, of course, not compete with a high-precision calculation optimized for a single electronic state. Fig. 1 demonstrates a comparison of the obtained electronic energies for different low-lying molecular states with high-precision calculations of L. Wolniewicz and co-workers performed using an explicitly correlated basis [42, 43, 44, 45, 46]. (The present CI method is able to reproduce such practically exact electronic energies at least within 4-6 significant digits, if the basis set is chosen judiciously [41]). The agreement is excellent for all states except for $1^1\Sigma_g^+$ and $1^1\Sigma_u^+$ (at larger internuclear distances) where the electronic motion is highly correlated and cannot efficiently be described by a CI calculation

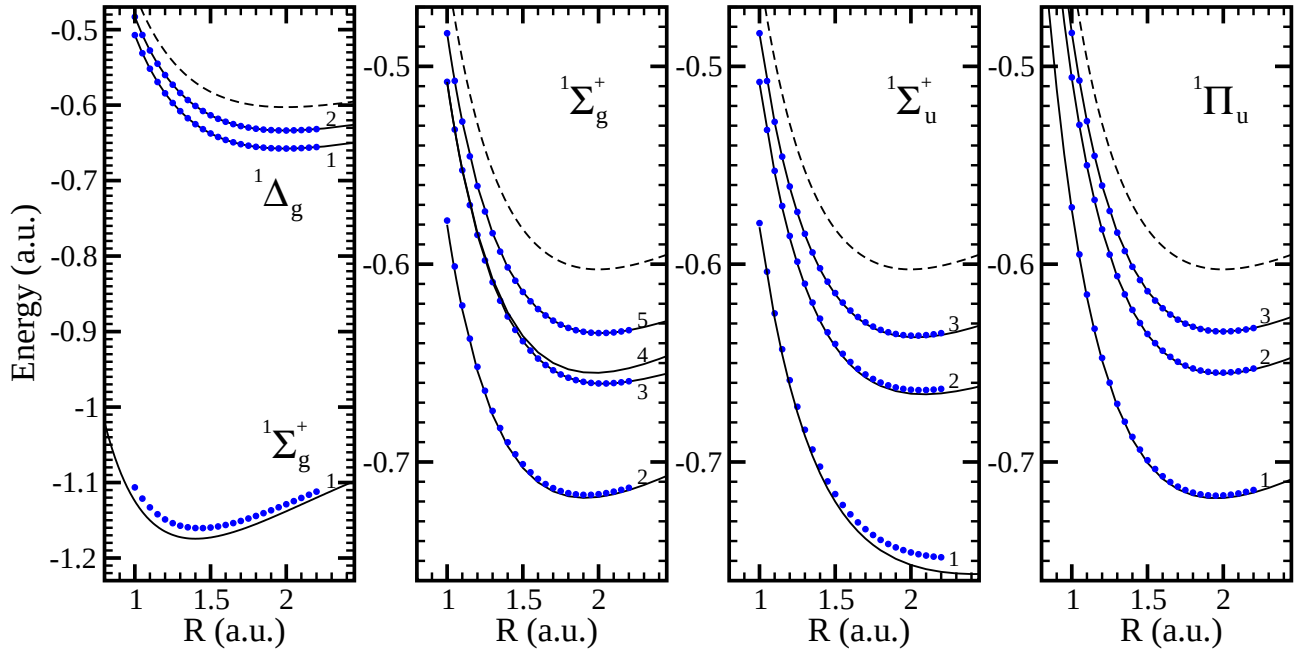

FIG. 1: Electronic potential curves of some low-lying states of H_2: the CI results of this work (blue circles) are compared to the supposedly exact values (solid lines, [42, 43, 44, 45, 46]). The dashed line shows the ionization threshold of H_2. The different adiabatic electronic states of a given molecular symmetry are numbered in the order of the energy.

employing orbitals with no electron-electron interaction included. Nevertheless, even for these two states the obtained electronic energies are much better than those obtained with the Hartree-Fock approximation. For example, for the ground state of H_2 with the exact electronic energy at $R = 1.4\,a_0$ being equal to -1.1745 a.u., the Hartree-Fock limit is -1.1336 a.u., whereas the present CI calculation yields -1.1604 a.u.

B. Integration over internuclear separations

Once the TDSE is solved for a given linear-polarized laser pulse, fixed internuclear separation R, and angle θ between the internuclear and the polarization axis, the ionization yield $Y_{\rm ion}(R,\theta)$ is obtained from a summation over the populations of all discretized continuum states. These yields can be further used to calculate the ionization yield $Y_{\rm ion}^{(\nu)}(\theta)$ for a given initial vibrational state ν described by the vibrational wavefunction $\phi_\nu(R)$. Indeed, if the duration of the pulse is sufficiently short and depletion of the state during the pulse is insignificant, one can neglect the motion of the wavepacket created during the pulse and calculate the total ionization yield as [34]

$$Y_{\rm ion}^{(\nu)}(\theta) = \int {\rm d}R\, Y_{\rm ion}(R,\theta)\,|\phi_\nu(R)|^2 \quad . \qquad (1)$$

Application of Eq. (1) is further based on the assumption that the molecule has no time to rotate during the pulse and neglect distortion of the electronic ground-state potential curve due to the external field. The latter assumption implies that the index ν of vibrational state should be sufficiently small. In this work, only $\nu = 0$ is considered, but for the two isotopes H_2 and D_2 with their different vibrational wavefunctions. Due to the larger mass the D_2 vibrational ground state is more compact than the one of H_2.

C. Atomic model

For the analysis of the orientational dependence of the ionization due to the anisotropy of a molecule, it is convenient to compare the molecular results with those obtained for an artificial atom with an isotropic, single-centered charge distribution. Strong-field ionization is, however, known to be not only sensitive to the symmetry, but also to the electronic binding energy and the exact form of the long-ranged Coulomb potential. Therefore, the artificial atom must agree to the corresponding molecule with respect to the two latter factors. For this reason the simple single-electron one-parameter model potential

$$V(r) = -\frac{1}{r}\left\{1 + \frac{\alpha}{|\alpha|}\exp\left[-\frac{2r}{|\alpha|^{1/2}}\right]\right\} \qquad (2)$$

was introduced [26]. Its performance for describing various physical problems was checked in [47] and it was recently also applied to the calculation of antiproton–H_2 scattering cross sections and stopping powers [48, 49].

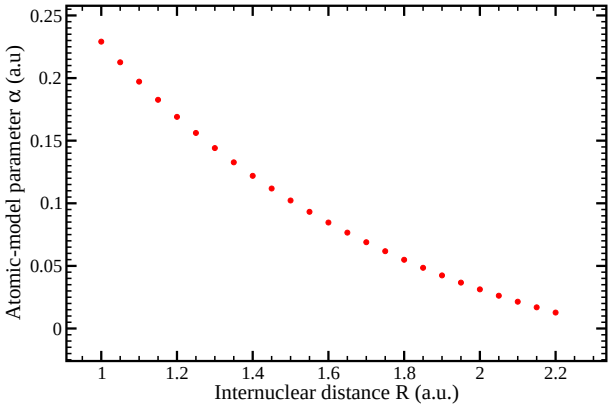

FIG. 2: Dependence of the atomic-model parameter α [see Eq. (2)] on the internuclear distance R. This choice of $\alpha(R)$ leads to a vertical ionization potential of H_2 in agreement with the one of the present CI calculation.

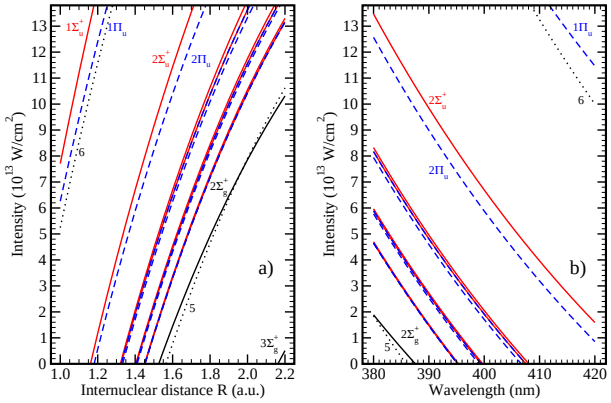

FIG. 3: Expected positions of REMPI peaks and N-photon ionization thresholds. Dependence of the resonant intensities I (a) on the internuclear distance R for pulses with a wavelength of 400 nm and (b) on wavelength for the fixed internuclear distance $R = 1.4\,a_0$. Positions of REMPI peaks due to Σ_u^+ (red solid), Π_u (blue dashes), or Σ_g^+ (black solid) intermediate states are shown. Also shown are the N-photon ionization thresholds (dotted lines, with N explicitly indicated in the graph).

The ionization potential I_p of such an artificial atom is directly related to the parameter α of the model potential (2). For a given ionization potential I_p the corresponding parameter α can be found as $\alpha = \alpha(I_p)$, where $\alpha(I_p)$ can be obtained numerically. Since the molecular vertical ionization potential (energy difference between the electronic ground-state potential curves of the ion and the neutral) depends on the internuclear distance R, the value of α should also depend on R in order to compare atomic-model and molecular results. Figure 2 shows the R dependence of α. It is determined by requiring the resulting R-dependent ionization potential to agree with the one obtained by the present CI calculation for the H_2 ground state.

In order to compare to the full molecular calculations the atomic-model results are multiplied by a factor 2 that accounts for the two equivalent electrons in molecular hydrogen. This procedure is known to be reasonable for ionization yields less than 10-20% [26] which is the case for the present calculations.

III. RESULTS

All calculations presented in this work were performed with N-cycle $\cos^2$-shaped linear-polarized laser pulses with $N = 10, 20$, and 40. For a wavelength of 400 nm the FWHM of intensity of such pulses corresponds to about 5, 10, and 20 fs.

A. Field-induced resonances

For the following discussion of the orientation dependence and isotope effects, it is helpful to obtain a more detailed understanding of the influence of such parameters as peak intensity and wavelength of the pulse or of the internuclear separation on the positions of REMPI peaks and N-photon ionization thresholds. In order to be able to correctly predict REMPI through some resonant electronic state in intense laser pulses, it is necessary to know the field-induced shift of the resonant state, what is a challenging task by itself. However, if the field is sufficiently intense, one can assume that the field-induced shift (dynamically induced Stark shift) of excited states is almost equal to the ponderomotive energy. With this assumption and using the field-free transition energies of the present CI calculation the positions of the REMPI peaks are expected to depend on the laser parameters and internuclear separation as shown in Fig. 3.

The dependence of the expected positions of the REMPI peaks and N-photon ionization thresholds on the internuclear distance R for a 400 nm laser field is given in Fig. 3 a. In this R range the ionization process can be referred to as 5-photon (7-photon) ionization in the bottom-right (top-left) part of the figure, or as 6-photon ionization otherwise. Different kinds of REMPI peaks are expected: (5+1) REMPI peaks through $n\Sigma_u^+$ or $n\Pi_u$ electronic states with $n > 1$, (5+2) REMPI peaks through the $1\Sigma_u^+$ or $1\Pi_u$ states, a (4+1) REMPI peak through the $3\Sigma_g^+$ state, and a REMPI peak through the $2\Sigma_g^+$ state. Note, that in the last case the expected position of the resonance crosses the expected position of the 5-photon ionization threshold. Therefore, the resonance can be referred to as (4+1) REMPI for peak intensities smaller than 7.5×10^{13} W/cm^2, and as (4+2) REMPI for higher intensities. Evidently, the correct character of the resonance is sensitive to the exact intensity dependence of the field-induced shift of the $2\Sigma_g^+$ state, and thus a non-trivial behavior is expected. A similar conclusion is

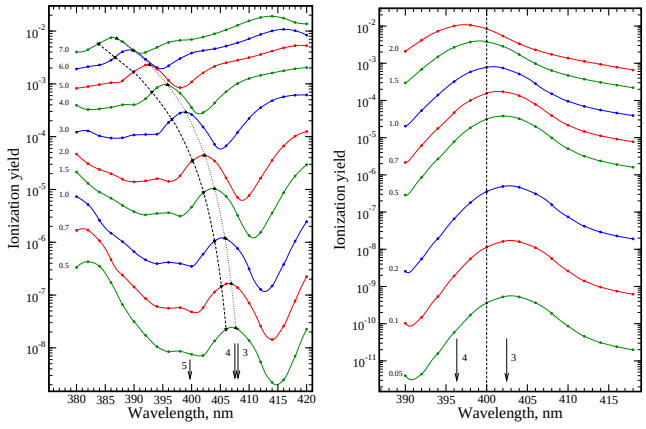

(a) $R = 1.4\,a_0$ (b) $R = 2.2\,a_0$

FIG. 4: Wavelength-dependent ionization yields for a parallel orientation of an H_2 molecule at the fixed internuclear distances (a) $R = 1.40\,a_0$ and (b) $R = 2.20\,a_0$ for various peak intensities (specified in units of 10^{13} W/cm^2) of 40-cycle cos^2-shaped pulses. The arrows indicate the resonant wavelengths (in the low-intensity limit) of REMPI peaks due to $n\Sigma_u^+$ (a) and $n\Sigma_g^+$ (b) intermediate states. The expected (dashes) and found (dots) position of a REMPI peak is also given in (a).

valid for the REMPI through the $1\Sigma_u^+$ or $1\Pi_u$ electronic states, since their exact REMPI positions could in fact cross the 6-photon ionization threshold.

Similarly, Fig. 3 b shows the dependence of expected positions of REMPI peaks and N-photon ionization thresholds on the laser wavelength for the fixed internuclear distance $R = 1.4\,a_0$. With larger peak intensity the increasing ponderomotive energy leads to an increase of the transition energy between the initial and the resonant state. This increase can be compensated by the increase of the photon energy, and thus the new REMPI position will occur at a smaller wavelength. The calculations at a fixed internuclear separation are more suitable for the investigation of the validity of the assumed field-induced shift of electronic states, since in this case identical sets of field-free electronic wavefunctions are used in the time propagation. For this purpose, a series of 210 calculations for a parallel-oriented H_2 molecule with fixed internuclear distance $R = 1.4\,a_0$ exposed to laser pulses with a total duration of 40 cycles was performed for 21 different values of the wavelength and 10 different values of the peak intensity. The results are shown in Fig. 4 a, where every point represents the outcome of one full TDSE calculation, and curves join the results obtained for the same peak intensity.

Figure 4 a shows a pronounced peak whose position moves from 407 nm for a peak intensity of 5×10^{12} W/cm^2 to 387 nm for a peak intensity of 7×10^{13} W/cm^2. From Fig. 3 b it follows that this peak can be assigned to REMPI through either one or both of the closely lying $3\Sigma_u^+$ and $4\Sigma_u^+$ electronic states, since the spectral width of the Fourier-limited pulse is too broad to resolve these two resonances. Clearly, the intensity-dependent shift of the peak position is overestimated by the already mentioned simple prediction based purely on the ponderomotive energy ($\delta E(I) = U_p$). Instead, the found intensity dependence of the field-induced energy shift can be well fitted by $\delta E(I) = 0.9U_p - 0.002$. At intensities 5×10^{12} W/cm^2 and smaller it appears as the energy shift of these low-lying excited states (responsible for the REMPI) is already absent. The position of the REMPI peak agrees then much better with the low-intensity limit than with the prediction based on U_p, since the latter would predict a shift of about 2 nm. Such a shift by about 2 nm is, however, found for the (poorly resolved) REMPI peak due to the higher lying $5\Sigma_u^+$ intermediate state. This demonstrates that in the investigated regime of laser parameters different excited states behave differently, and a common prediction for all excited states is impossible.

Figure 4 b shows again the results of a series of (this time 120) calculations for a parallel-oriented H_2 molecule, but for the larger internuclear separation $R = 2.2\,a_0$. In this case the spacing of the $3\Sigma_g^+$ and $4\Sigma_g^+$ states that could lead to (4+1) REMPI is rather large, and thus the pronounced peak in Fig. 4 b can be entirely assigned to REMPI through the $3\Sigma_g^+$ state. Although the peak position clearly shifts to smaller wavelengths with increasing laser peak intensity, the shift becomes visible only for rather large intensities. As a consequence, the peak position crosses 400 nm at an intensity higher than 10^{13} W/cm^2, whereas according to Fig. 3 a the crossing should have occurred at an intensity that is smaller by a factor 2. Thus, although the positions presented in Fig. 3 give a satisfactory explanation of the main features, they should only be considered as a rough estimate.

B. R-dependent ionization

If strong-field ionization of H_2 or D_2 initially in their vibrational ground states is considered, it is important to investigate the dependence of the ionization on the internuclear separation R within an R range in which the vibrational wave function is nonvanishing (Franck-Condon window). Therefore, the TDSE describing H_2 within the fixed-nuclei approximation was solved for 25 different values of R (in between $1.0\,a_0$ and $2.2\,a_0$ with a step size of $0.05\,a_0$). This was repeated for 15 different values of peak intensities (in a range from 2×10^{13}W/cm^2 to 1.3×10^{14}W/cm^2).

Figure 5 a (left panel) shows the obtained results for a parallel orientation of the molecular axis with respect to the polarization vector and 40-cycle cos^2-shaped (FWHM of about 20 fs) laser pulses. Two main features may be observed. First, the ionization yield increases with R. Second, pronounced structures are visible. The importance of both effects decreases with intensity. The increase with R was first predicted in the quasistatic regime [34]. Its occurrence at 400 nm shows that even for this wavelength clear strong-field phenomena are observable

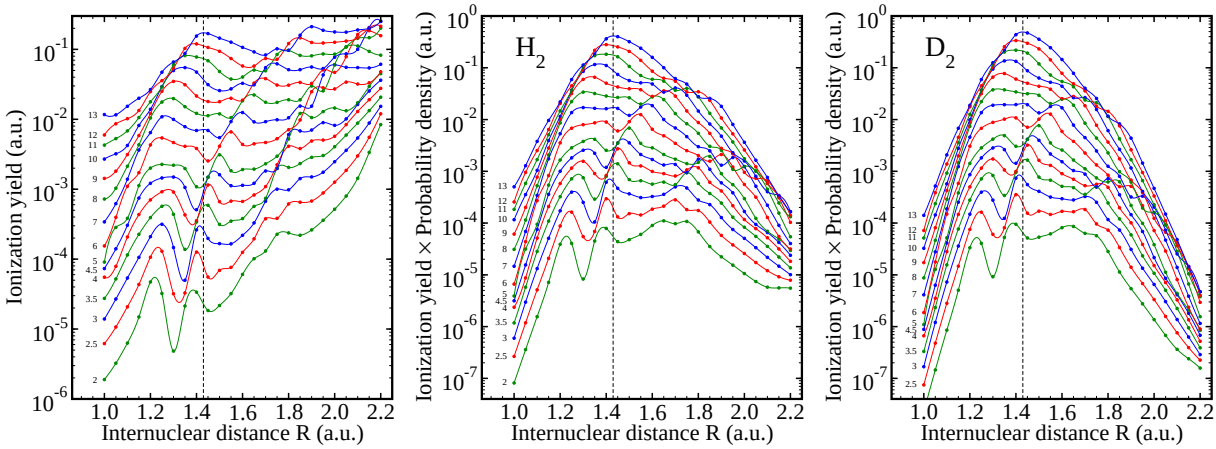

(a)Parallel orientation of the internuclear axis to a linear polarized laser field

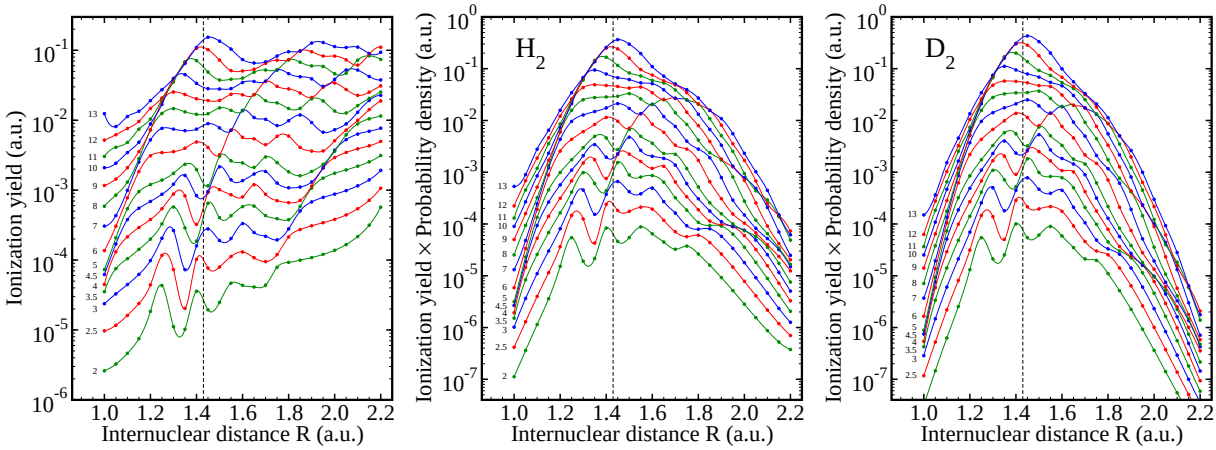

(b)Perpendicular orientation of the internuclear axis to a linear polarized laser field

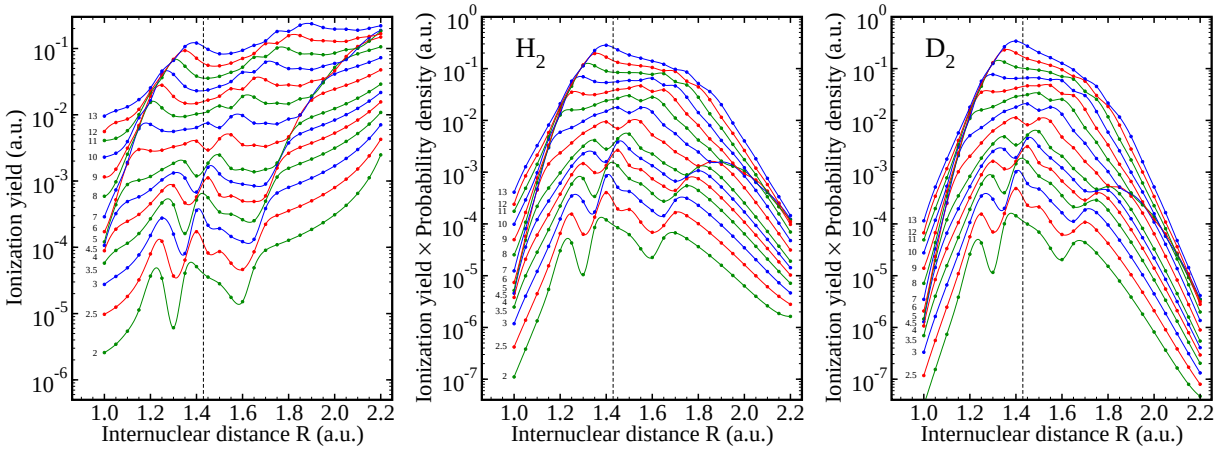

(c)Atomic model calculations (multiplied by a factor 2)

FIG. 5: Ionization yields for 40-cycle $\cos^2$-shaped (20 fs) laser pulses with a wavelength of 400 nm and different peak intensities in between 2.0 and 13×10^{13} W/cm^2 (specified in the graphs in units of 10^{13} W/cm^2). The upper (middle) panel shows the results for a parallel (perpendicular) orientation of the molecule with respect to the field axis, while the lower panel shows the results obtained with the atomic model potential in Eq. (2). The left panel shows the fixed-nuclei ionization yields as a function of the internuclear distance R, whereas the middle and right panels display the ionization yields multiplied with the probability density of the ground vibrational states of H_2 and D_2, respectively. (Every point corresponds to a full solution of the TDSE, while the points are connected by spline interpolating curves.)

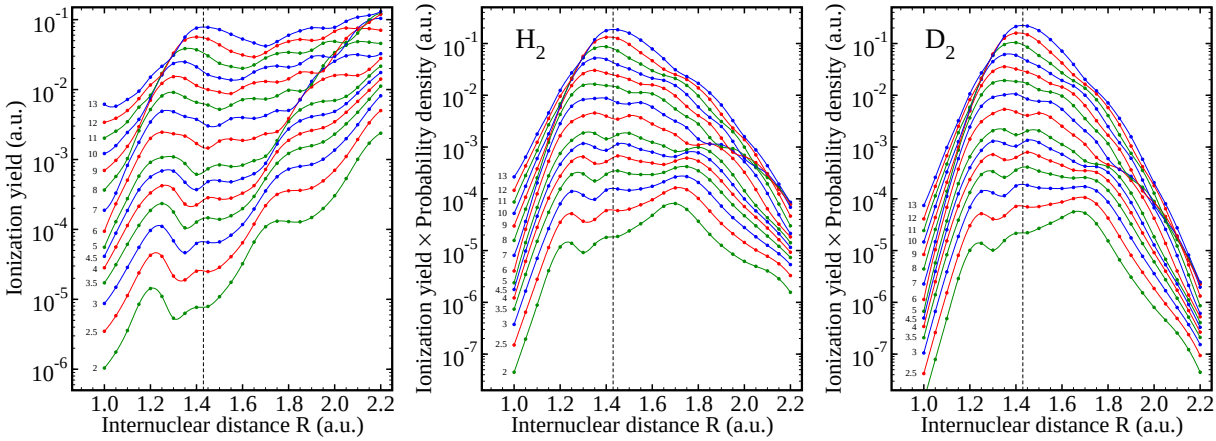

(a)Parallel orientation of the internuclear axis to a linear polarized laser field

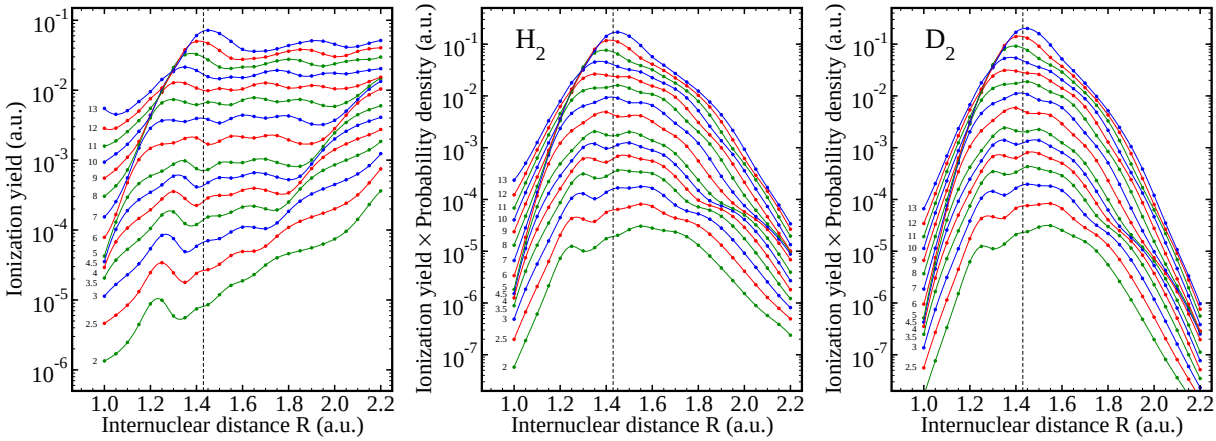

(b)Perpendicular orientation of the internuclear axis to a linear polarized laser field

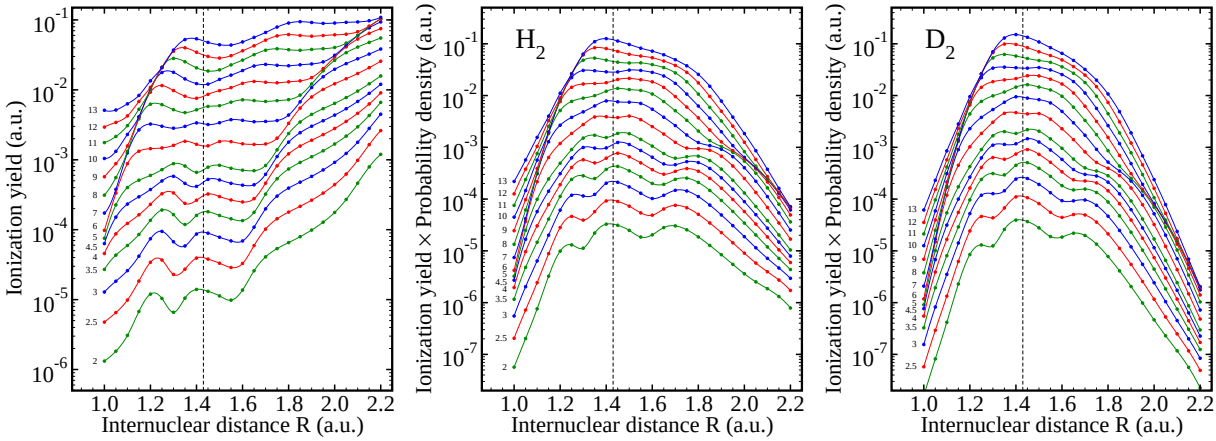

(c)Atomic model calculations (multiplied by a factor 2)

FIG. 6: As Figure 5, but for a 20-cycle $\cos^2$-shaped (10 fs) laser pulse.

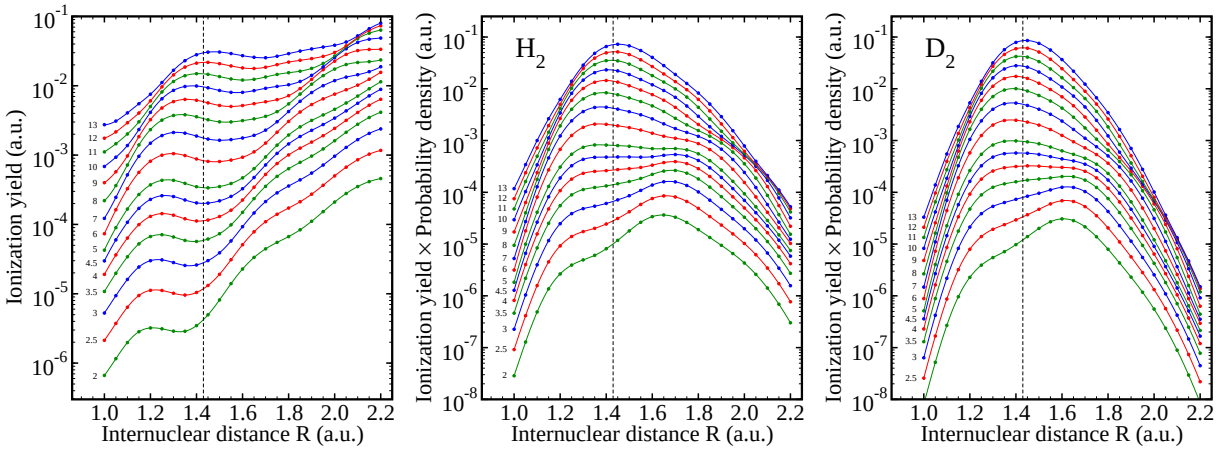

(a)Parallel orientation of the internuclear axis to a linear polarized laser field

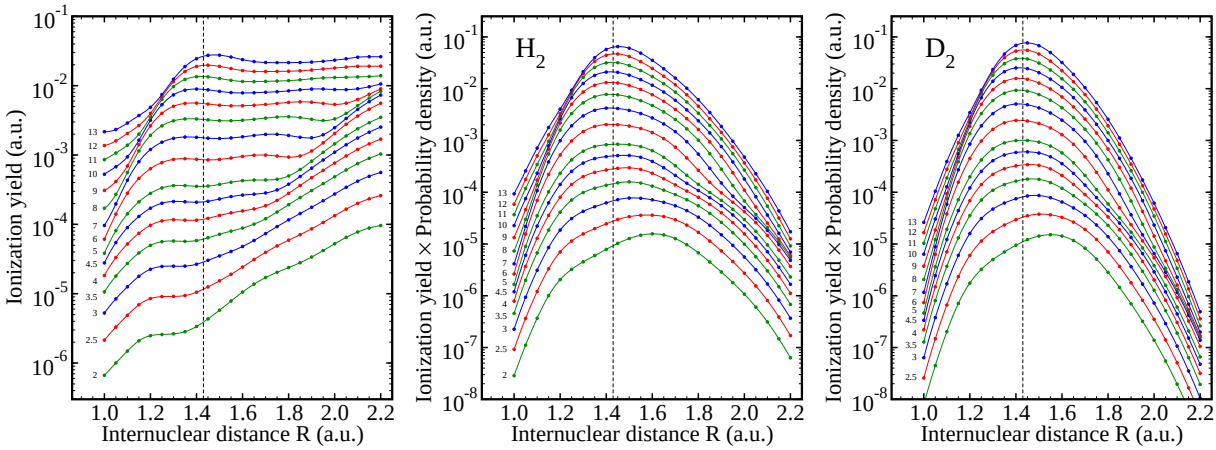

(b)Perpendicular orientation of the internuclear axis to a linear polarized laser field

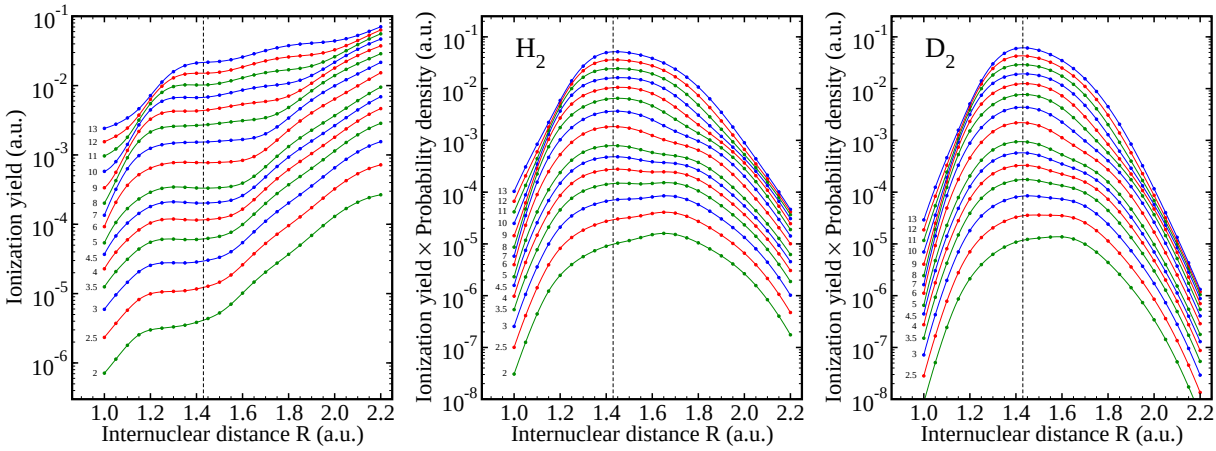

(c)Atomic model calculations (multiplied by a factor 2)

FIG. 7: As Figure 5, but for a 10-cycle $\cos^2$-shaped (5 fs) laser pulse.

beyond a pure multiphoton picture. On the other hand, the observed structures are due to classical multiphoton phenomena (channel closings and REMPI).

Some pronounced REMPI peaks are visible that should be compared with their predicted positions in Fig. 3. The peaks at $R = 1.2\,a_0$ and $R = 1.4\,a_0$ for a laser peak intensity of 2×10^{13}W/cm^2 can thus be assigned to (5+1) REMPI through the $2\,\Sigma_u^+$ and $3 - 4\,\Sigma_u^+$ states, respectively. The position of the latter peak changes with the peak intensity almost in the expected way as has

also been demonstrated in Fig. 4 a. On the other hand, the position and amplitude of the REMPI peak arising from the $2\,\Sigma_u^+$ resonant state cannot easily be understood. For a peak intensity of 10^{14}W/cm^2 this REMPI peak is located at $R = 1.6\,a_0$ instead of the expected value of $1.5\,a_0$. Interestingly, the amplitude of the peak that is very large at small intensities is becoming very small for higher intensities, as one may expect when going from the multiphoton in the direction of the quasistatic regime. For intensities between 4×10^{13}W/cm^2 and 6×10^{13}W/cm^2 one can observe something similar to a splitting of the REMPI peak into two peaks. This behavior can evidently not be explained using Fig. 3. It is also difficult to explain the pronounced peak located at $R = 1.4\,a_0$ for the highest laser peak intensity (1.3×10^{14}W/cm^2). According to Fig. 3 no peak should occur for these values of R and I, since it lies in between the expected positions of the $1\,\Sigma_u^+$ and the $2\,\Sigma_u^+$ REMPI peaks. This may indicate some field-induced coupling of these states and thus a clear strong-field phenomenon. It is also interesting to note that the channel closings indicating the transitions from 5- to 6-photon ionization and from 6- to 7-photon ionization are visible, but not very pronounced. Furthermore, due to the REMPI peaks the channel thresholds are sometimes difficult to identify in the shown ionization yields.

In order to consider the influence of vibrational motion onto the strong-field ionization yields, the results obtained for a fixed nuclear orientation are weighted with the probability density of the ground vibrational state [see integrand of Eq. (1)]. The corresponding result for H_2 is shown in the middle panel of Fig. 5. Only in the case of the highest laser peak intensity considered in this work, the maximum of the weighted ionization yield agrees with the maximum of the vibrational wave function. At slightly lower intensities (until about 8×10^{13}W/cm^2) the weighted ionization yield is largest for smaller values of R, while for even lower intensities the REMPI peaks due to the $3\,\Sigma_u^+$ and $4\,\Sigma_u^+$ states determine the maximum of the weighted ionization yield. At the lowest laser peak intensity considered (2×10^{13}W/cm^2) the highest weighted ionization yield is found at around $R = 1.7\,a_0$. This maximum should be due to an opening of the 5-photon regime and may be further increased by (4+1) REMPI processes. At this intensity one notices also a very slow decrease of the weighted ionization yield for R values above $2\,a_0$, despite the fact that the vibrational wave function has a very small amplitude. The reason is the already discussed $3\,\Sigma_g^+$ REMPI peak (Fig. 4 b).

In the case of D_2 (left panel of Fig. 5 a) the narrower vibrational distribution is, however, sufficient to dominate over the resonant effect. In this case the weighted ionization yield decreases rather pronouncedly for internuclear separations larger than $2.0\,a_0$. Close to the minimum of the electronic potential curve at about $1.4\,a_0$ the weighted ionization yields are, however, very similar for H_2 and D_2. Also for D_2 the ionization yield peaks only for the highest intensity considered here at the maximum of the vibrational wavefunction. Consequently, the Franck-Condon approximation would not describe the vibrational distribution of the formed H_2^+ ions properly. A proper calculation of these distributions has to include the effects of channel closings and REMPI, but also of the general increase of the ion yield as a function of internuclear separation. Neither a pure multiphoton nor quasistatic prediction is thus sufficient.

C. Orientational dependence

For a perpendicular orientation of the molecule with respect to the field (Fig. 5 b) the R-dependent ionization yield (left panel) looks on the first glance surprisingly similar to the one for the parallel orientation. For the lowest shown intensities the spectra comprise very pronounced peaks at about $R = 1.25\,a_0$ and $R = 1.4\,a_0$ that can be assigned to (5+1) REMPI through the $2\,\Pi_u$ and the $3 - 4\,\Pi_u$ states, respectively. It is a peculiarity of H_2 that already the lowest lying excited states of $^1\Sigma_u$ and $^1\Pi_u$ symmetry and thus REMPI peaks through those states lie energetically very close together. In contrast to the results for parallel orientation a third peak at $R = 1.55\,a_0$ is, however, also well resolved. From Fig. 3 it appears very likely that this peak stems from a superposition of (5+1) REMPI processes through the higher excited Π_u states. Especially at lower intensities one notices furthermore that the ionization yield does not increase that evidently for large R values than it does for a parallel orientation. The threshold between 5- and 6-photon ionization is rather well resolved and appears for the different laser peak intensities more or less at the expected R values (Fig. 3 a). As a consequence of the smaller slope at large R the weighted ionization yield decays for larger R values much faster for the perpendicular than for the parallel orientation for both H_2 (middle panel of Fig. 5 b) and D_2 (right panel).

Figure 5 c shows finally the ionization yield obtained with the simple isotropic one-electron model potential given in Eq. (2). The agreement of the R-dependent ionization yields obtained with this model and the full molecular two-electron calculation are surprisingly good, especially with the results obtained for the parallel orientation. As in the latter case, the atomic model gives a shifted threshold between the 5-and 6-photon regimes compared to the prediction according to Fig. 3. The atomic model yields also a rather pronounced increase in ionization for large R values, especially for low laser peak intensities as was also found for the parallel orientation. A closer look reveals, however, that for small R separations and especially for the first REMPI peak the atomic model agrees slightly better with the molecular results obtained for the perpendicular orientation. The 2nd REMPI peak defines somehow the transition line. For smaller R values the atomic model agrees better with the perpendicular results, while starting with the 2nd REMPI peak the ionization yields obtained for the

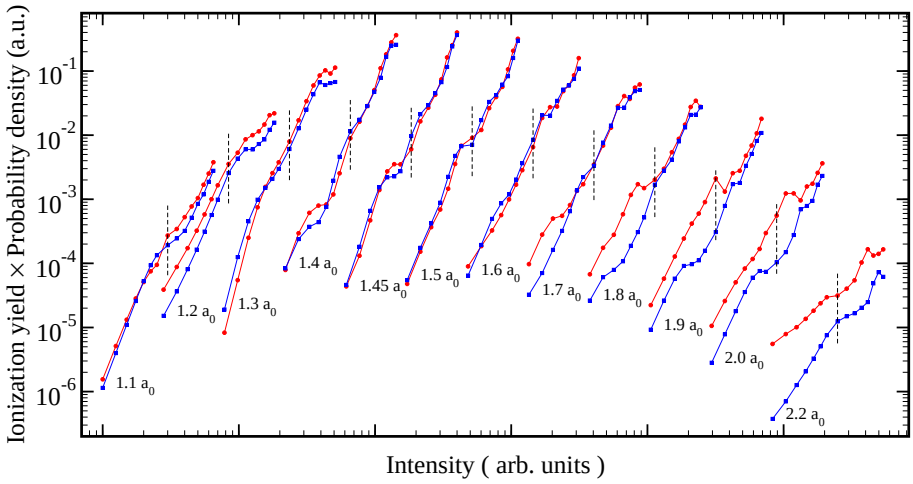

FIG. 8: Comparison of ionization yields (in a 20 fs laser pulse) for different internuclear distances R (weighted with the the probability density of the ground vibrational state of H_2 at this R) for a parallel (red curves) and a perpendicular (blue curves) oriented H_2 molecule. The R values are specified explicitly in the figure. The vertical dashed lines indicate the position of a peak intensity $6 \times 10^{13}\mathrm{W/cm^2}$ on the intensity axis for every corresponding pair of curves.

atomic model and the molecular one for a parallel orientation agree better with each other. The main difference to the molecular calculations is the position of the 3rd REMPI peak that for the lowest shown intensity lies so close to the 2nd one, that it appears in the R-dependent ionization yield as a shoulder. For a laser peak intensity of $2.5 \times 10^{13}\mathrm{W/cm^2}$ the 3rd REMPI peak is shifted more than the 2nd one and is thus visible as a well separated peak. However, for higher intensities it is less well resolved due to its low probability. Despite the overall good agreement of the results for the atomic model with the full molecular calculations (on a logarithmic scale!), the weighted ionization yields still reveal differences. For example, the maximum of the weighted ionization yields for H_2 and D_2 and the largest laser peak intensities is shifted to slightly smaller R values than is found for the full molecular calculations.

A further important laser parameter is the pulse duration. Its influence is demonstrated in Figs. 6 and 7 that show the corresponding results for 20- and 10-cycle pulses (FWHM of 10 and 5 fs), respectively. The increased laser bandwidth leads to spectra that show much less details compared to the relatively long 40-cycle pulse. The ionization yields for the 10-cycle pulse show almost no evidence of REMPI peaks. The curves are fairly smooth and the remaining structures can be explained by the closing and opening of N-photon ionization channels.

Because of the different positions of the REMPI peaks for parallel or perpendicular orientations the ratio of parallel to perpendicular ionization yields may substantially change for a small variation of R. This effect is demonstrated in Fig. 8 in which ionization yields (multiplied with the probability density of the ground vibrational state) for parallel and perpendicular oriented H_2 molecule are compared for different internuclear distances. A log-log scale is used and the pairs of curves (parallel and perpendicular orientation for a given value of R) are shifted along the intensity axis for better readability. To guide the eye, the vertical dashed lines indicate the position of the peak intensity $6 \times 10^{13}\mathrm{W/cm^2}$ on the intensity axis for every pair of curves. The multiplication with the probability density was performed in order to emphasize the relative contributions of different internuclear distances for the total ionization ratio between parallel and perpendicular orientations obtained after integration over R.

As can be seen from Fig. 8, the ionization yields for parallel and perpendicular orientation are almost equal in the range $R = 1.3 - 1.7\,a_0$ for a peak intensity of $6 \times 10^{13}\mathrm{W/cm^2}$. Whereas the ionization yield for the parallel orientation is larger than for the perpendicular one at $R = 1.3$ and $1.5\,a_0$, the opposite is found at $R = 1.4, 1.45$, and $1.6\,a_0$. At smaller values of R the parallel orientation is slightly easier ionized than the perpendicular one, while for R values larger than $1.8\,a_0$ parallel oriented molecules are much easier ionized. This is a consequence of the slower decay of the ionization yield for a parallel orientation and for large R values that was already discussed in the context of Figs. 5 a and b.

The key conclusion that can be drawn from Fig. 8 is the need for systematic studies of the intensity and internuclear-separation dependencies of the ratio between the ionization yields for parallel or perpendicular orientation as they are performed in this work, since a calculation for a single laser peak intensity and internuclear separation R can yield any possible result, i. e. the ratio between the ionization yields for parallel and perpendicular orientations may be found to be equal to 1, much smaller than 1, or much larger than 1. Depending on the choice of intensity and R very different conclusions

on the orientation dependence of the ionization yield of H_2 in strong laser fields would follow.

D. Integrated ionization yields

The R-independent ionization yields for H_2 and D_2 molecules (in their vibrational ground states) are finally obtained by an integration of the weighted R-dependent ionization yields over R (Eq. (1) in Sec. II B). The results for parallel and perpendicular orientation are shown for the different pulse lengths in Fig. 9. The curves obtained after R integration are much less structured than the fixed-nuclei ionization yields, as is evident from a comparison with Fig. 8). Clearly, the structures due to REMPI processes are smoothed out by the integration over R. As a consequence, the curves look almost like straight lines on the used log-log scale.

In fact, it turns out that the linear dependence on the logarithmic scale is well described, if the yield is fitted with the function

$$Y_s(I,T) = \Omega\, T\, (I/I_0)^{k_s} \tag{3}$$

where I is the peak intensity, $I_0 = 3.5094452 \times 10^{16}$ W/cm^2 is the atomic unit of intensity, and T is the FWHM duration of the pulse in atomic units. For the fit parameters the values $\Omega = 1.55 \cdot 10^6$ and $k_s = 4.17$ are found. The obtained value of k_s indicates a non-perturbative behavior, since according to Fig. 3 a one would expect mostly 6-photon ionization to occur and thus k_s should be close to 6. The included dependence on the pulse duration T allows to compare the results obtained for different pulse lengths. A linear dependence on T should be found, if a rate concept is applicable.

Dividing the ionization yields by the fit function (3) allows a direct comparison of the parallel, perpendicular, and atomic model potential results on a linear scale. They are shown in the inserts of Fig. 9. If the vibrational ground state of H_2 is considered (middle panel of Fig. 9), the scaled atomic-model results are closest to 1 and thus most accurately described by the fit function. The scaled yield for parallel orientation decreases from a value of 1.5 to about 1.0 for the 10-cycle pulse, but shows an increasing behavior for higher intensities in the case of the 20-cycle pulse. The smallest intensity dependence is found for the longest pulse considered in this work where the scaled yield varies only between about 1.25 and 1.15. Interestingly, the scaled yield for perpendicular orientation shows almost the opposite behavior. The most pronounced intensity dependence is found for the longest pulse. Furthermore, the scaled yield increases for low intensities as a function of intensity. As a consequence, the scaled yields for parallel and perpendicular orientation first approach each other before they separate again for even larger intensities.

Using the same fit function for scaling the D_2 yields one notices that the yields for parallel orientation are now almost flat (shortest pulse) or increase with intensity. Since the vibrational density distribution of D_2 is more localized around R_0, one can conclude that such higher ratio for H_2 can be due to contributions to the ionization from either small or large internuclear distances R. The comparison of the middle and the right panels of Fig. 7 a shows that the effect stems from the enhanced ionization at $R > 1.6\, a_0$. Also the scaled yields for perpendicular orientation or the atomic model potential show a larger increase with intensity for D_2 compared to H_2, although this effect is a little bit less pronounced. This indicates that the ionization yield of D_2 possesses a slightly larger slope than the one of H_2, a rather unexpected (though small) isotope effect.

Finally, the ratio of the ionization yields for parallel to perpendicular orientation of the molecular axis as a function of the peak intensity is also shown in Fig. 9. For the 10-cycle pulse and H_2 the ratio is about 2 for the peak intensity 2×10^{13}W/cm^2 and decreases smoothly to about 1.1 at 9×10^{13}W/cm^2, before it increases to 1.18 at 1.3×10^{14}W/cm^2. The occurrence of a minimum is due to the maximum found for scaled yield in the case of the perpendicular orientation, as was discussed in the context of the inserts in the middle and right panels of Fig. 9. Increasing the pulse duration does not change the behavior in a qualitative fashion, but the ratio found at small intensities decreases with increasing pulse length. At the same time, the increase at the highest intensities is more pronounced, but this increase is smaller than the decrease seen for the low intensities. In the case of the 40-cycle pulse the ratio starts at about 1.5, decreases to almost 1.0 and increases to 1.26. The turning point shifts also to slightly lower intensities for longer pulses. The intensity dependence of the ratios for D_2 show a similar behavior as was found for H_2. However, at small intensities the ratio is clearly smaller than for H_2, i. e. the anisotropy of the ionization yield is less pronounced. For high intensities the ratios found for H_2 and D_2 agree on the other hand almost perfectly with each other. An isotope effect occurs thus only for low intensities.

The importance of the inclusion of nuclear motion is evident from the ratio of parallel to perpendicular ionization yields obtained for a fixed internuclear separation ($R = 1.4\, a_0$) that is also shown in Fig. 9. In the case of a 10-cycle pulse the ratio is also smooth, but increases with intensity. The pronounced decrease found for the R-integrated ratio at low intensities is thus completely absent. Interestingly, the agreement with the ratio found for H_2 is very good for high intensities for which also the H_2 and D_2 ratios agreed well with each other. This indicates that for high intensities the ratio is less sensitive to R. The reason is the less pronounced R dependence of the ionization yields for high intensities that was found in general and discussed in the context of the weighted R-dependent ionization yields in Figs. 5 to 7. One of the consequences of this reduced R dependence was, e. g., that the maximum of the ionization yield was more or less found for the R value at which the vibrational density had its maximum. For longer pulses pronounced

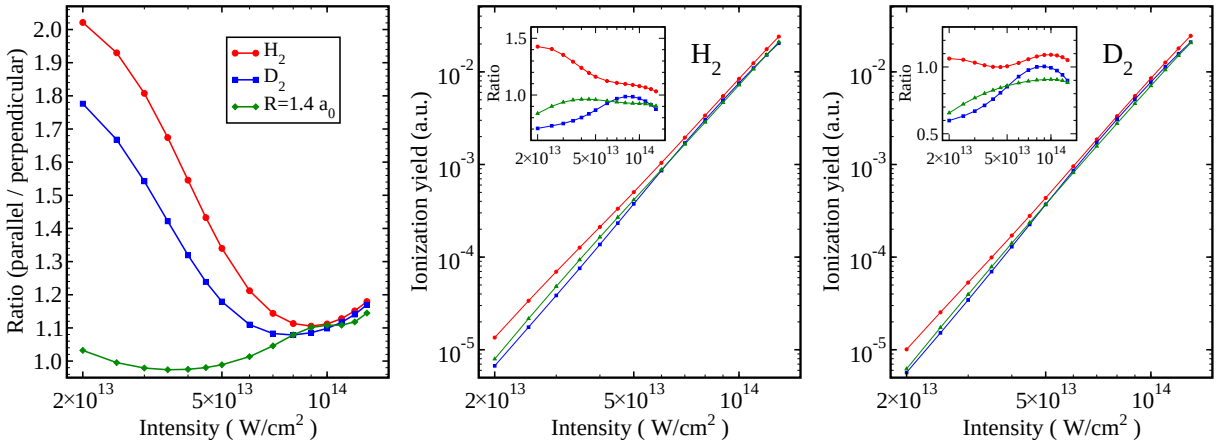

(a)10-cycle cos^2-shaped (5 fs) laser pulse

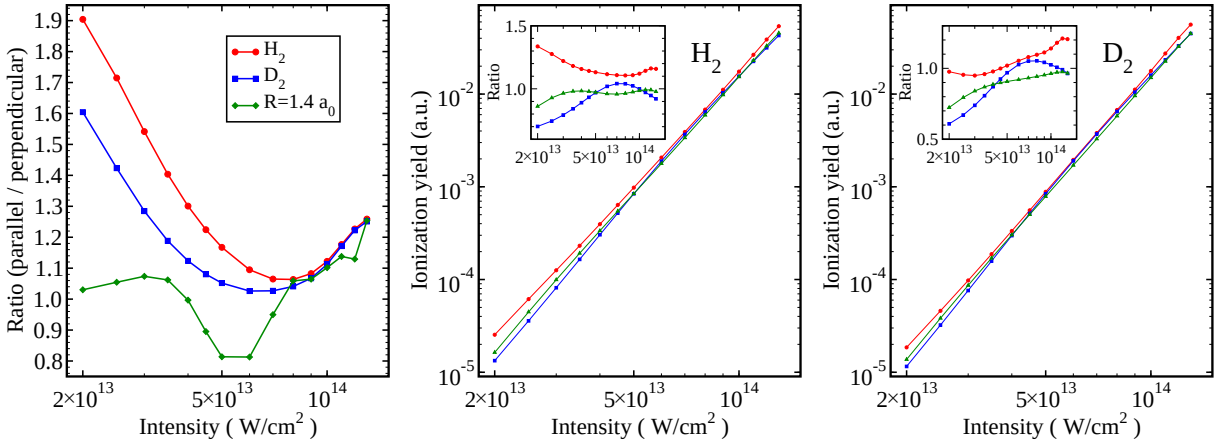

(b)20-cycle cos^2-shaped (10 fs) laser pulse

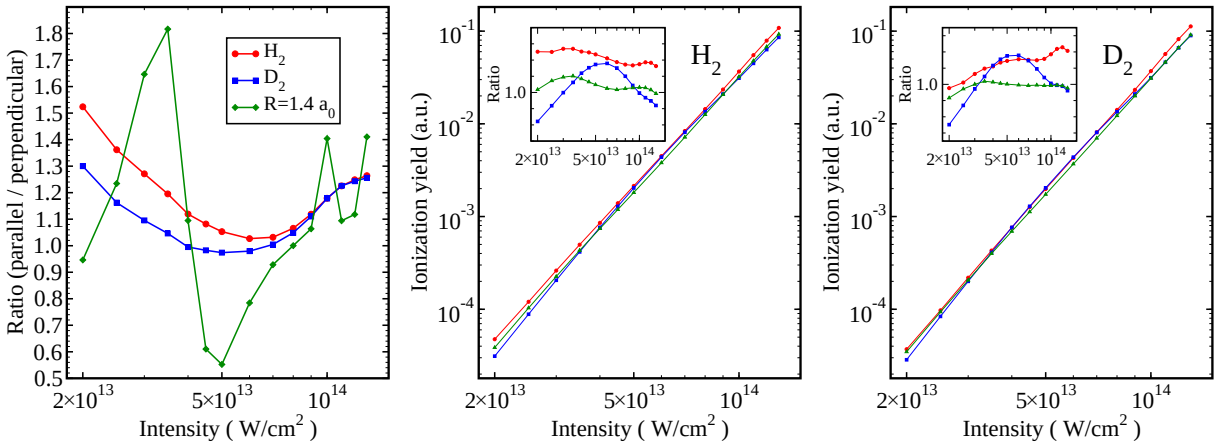

(c)40-cycle cos^2-shaped (20 fs) laser pulse

FIG. 9: Final ionization yields (integrated over the internuclear separation R) as a function of the laser peak intensity for H_2 (middle panel) and D_2 (right panel) and a parallel (red circles) or a perpendicular (blue squares) orientation and a) 10-cycle, b) 20-cycle, or c) 40-cycle laser pulses. Also shown are the results obtained with the isotropic one-electron model potential (green triangles). The inserts show the ratio of the ionization yields to the fit function in Eq. (3). The resulting ratio of parallel to perpendicular ionization yields is shown in the left panel in which also the corresponding ratio obtained for a fixed internuclear separation ($R = 1.4\,a_0$) is plotted.

intensity-dependent maxima and minima become visible. As a consequence, the ratio found for a single R value differs clearly from the R-integrated results. For example, in the case of a 40-cycle pulse and $R = 1.4\,a_0$ the ratio decreases to about 0.5 at a laser peak intensity of $5\times10^{13}\mathrm{W/cm^2}$ which means that perpendicular oriented H_2 ionizes much better than parallel oriented one. This is in complete contrast to the R-integrated results for which the perpendicular orientation never ionizes faster than parallel oriented molecules in the considered range of laser peak intensities.

IV. CONCLUSION

We have performed an extensive numerical study of intense-field ionization of molecular hydrogen and deuterium numerically integrating the full-dimensional two-electron Schrödinger equation in the non-relativistic, fixed-nuclei, and dipole approximation. The presented results are obtained for three different durations $(5, 10, 20\,\mathrm{fs})$ of ultrashort frequency-doubled Ti:sapphire laser pulses (400 nm) for both parallel and perpendicular orientations of the molecular axis with respect to the laser field. Calculations are performed for 15 different intensities (in a range from $2\times10^{13}\,\mathrm{W\,cm^{-2}}$ to $1.3\times10^{14}\,\mathrm{W\,cm^{-2}}$) and 25 different internuclear separations (in a range from $1.0\,a_0$ to $2.2\,a_0$) which results in 375 data points for each orientation. The same series of calculations was performed employing an isotropic one-electron model potential in order to study the influence of molecular anisotropy or the one of the two electrons.

By analyzing the dependence of the fixed-nuclei ionization yields on the peak intensity and the internuclear separation, we assign the observed peaks to REMPI or closings of N-photon ionization channels and study field-induced shifts of resonant electronic states.

A key feature of the present work is the calculation of total ionization yields of molecular hydrogen and deuterium in their ground vibrational states by an integration of the fixed-nuclei ionization yields multiplied with the corresponding vibrational probability density over the internuclear separation. The subsequent analysis of the ionization anisotropy reveals a smooth dependence on the laser peak intensity and pulse duration. The obtained ratios of the parallel to perpendicular total ionization yields vary in the investigated intensity and pulse duration ranges in between 1 and 2. Whereas for high intensities the ionization anisotropy of H_2 and D_2 is almost identical, the ratio for H_2 is always larger than the one for D_2 in the case of small intensities, although the difference does not exceed 20 %.

The importance of the integration over the internuclear separation for the interpretation of experiments is demonstrated by comparing the obtained parallel to perpendicular ratios with those calculated using the fixed-nuclei results at the equilibrium distance. For example, there is a wide range of intensities where at the equilibrium distance the ionization for perpendicular-oriented molecule is larger than for parallel-oriented ones. Besides the rather different qualitative dependence on the peak intensity, also the dependence on the pulse duration is different.

The results of this work do not only provide an interesting insight into the strong-field behavior of molecules and the influence of channel closings, REMPI, field-induced shifts of energy positions, pulse length and intensity, vibrational motion, isotope effects, and orientation, but will hopefully also stimulate experimental efforts to measure the anisotropy of the ionization yield of H_2 (or D_2) in the interesting regime that is neither well described by the multiphoton nor the quasistatic approximations. Furthermore, the results should serve as benchmarks for other theoretical approaches and simplified models.

Acknowledgments

This work was supported by the Deutsche Forschungsgemeinschaft (Sa936/2) and COST action CM0702. AS is grateful to the Stifterverband für die Deutsche Wissenschaft (Program "Forschungsdozenturen") and the Fonds der Chemischen Industrie for financial support.

[1] J. H. Posthumus, Rep. Prog. Phys. **67**, 623 (2004).
[2] I. V. Hertel1 and W. Radloff, Rep. Prog. Phys. **69**, 1897 (2006).
[3] J. Itatani, J. Levesque, D. Zeidler, H. Niikura, H. Pépin, J. C. Kieffer, P. B. Corkum, and D. M. Villeneuve, Nature **432**, 867 (2004).
[4] M. Meckel, D. Comtois, D. Zeidler, A. Staudte, D. Pavičić, H. C. Bandulet, H. Pépin, J. C. Kieffer, R. Dörner, D. M. Villeneuve, et al., Science **320**, 1478 (2008).
[5] J. J. Larsen, H. Sakai, C. P. Safvan, I. Wendt-Larsen, and H. Stapelfeldt, J. Chem. Phys. **111**, 7774 (1999).
[6] H. Stapelfeldt and T. Seideman, Rev. Mod. Phys. **75**, 543 (2003).
[7] I. V. Litvinyuk, K. F. Lee, P. W. Dooley, D. M. Rayner, D. M. Villeneuve, and P. B. Corkum, Phys. Rev. Lett. **90**, 233003 (2003).
[8] D. Zeidler, A. B. Bardon, A. Staudte, D. M. Villeneuve, R. Dörner, and P. B. Corkum, J. Phys. B: At. Mol. Phys. **39**, L159 (2006).
[9] D. Pavičić, K. F. Lee, D. M. Rayner, P. B. Corkum, and D. M. Villeneuve, Phys. Rev. Lett. **98**, 243001 (2007).
[10] A. Staudte, S. Patchkovskii, D. Pavičić, H. Akagi, O. Smirnova, D. Zeidler, M. Meckel, D. M. Villeneuve, R. Dörner, M. Y. Ivanov, et al., Phys. Rev. Lett. **102**, 033004 (2009).

[11] M. Magrakvelidze, F. He, S. De, I. Bocharova, D. Ray, U. Thumm, and I. V. Litvinyuk, Phys. Rev. A **79**, 033408 (2009).
[12] A. Jaroń-Becker, A. Becker, and F. H. M. Faisal, Phys. Rev. A **69**, 023410 (2004).
[13] T. K. Kjeldsen and L. B. Madsen, Phys. Rev. A **73**, 047401 (2006).
[14] D. B. Milošević, Phys. Rev. A **74**, 063404 (2006).
[15] V. I. Usachenko, Phys. Rev. A **73**, 047402 (2006).
[16] D. A. Telnov and S.-I. Chu, Phys. Rev. A **79**, 041401(R) (2009).
[17] I. A. Bocharova, H. Mashiko, M. Magrakvelidze, D. Ray, P. Ranitovic, C. L. Cocke, and I. V. Litvinyuk, Phys. Rev. A **77**, 053407 (2008).
[18] T. Wilbois and H. Helm, Laser Phys. **18**, 579 (2008).
[19] K. Harumiya, I. Kawata, H. Kono, and Y. Fujimura, J. Chem. Phys. **113**, 8953 (2000).
[20] M. Awasthi, Y. V. Vanne, and A. Saenz, J. Phys. B: At. Mol. Phys. **38**, 3973 (2005).
[21] A. Palacios, H. Bachau, and F. Martín, Phys. Rev. Lett. **96**, 143001 (2006).
[22] A. Apalategui and A. Saenz, J. Phys. B: At. Mol. Phys. **35**, 1909 (2002).
[23] M. Uhlmann, T. Kunert, and R. Schmidt, J. Phys. B: At. Mol. Phys. **39**, 2989 (2006).
[24] L. A. A. Nikolopoulos, T. K. Kjeldsen, and L. B. Madsen, Phys. Rev. A **76**, 033402 (2007).
[25] M. Awasthi, Y. V. Vanne, A. Saenz, A. Castro, and P. Decleva, Phys. Rev. A **77**, 063403 (2008).
[26] Y. V. Vanne and A. Saenz, J. Mod. Opt. **55**, 2665 (2008).
[27] H. Niikura, F. Légaré, R. Hasbani, A. D. Bandrauk, M. Y. Ivanov, D. M. Villeneuve, and P. B. Corkum, Nature **417**, 917 (2002).
[28] H. Niikura, F. Légaré, R. H. M. Y. Ivanov, D. M. Villeneuve, and P. B. Corkum, Nature **421**, 826 (2003).
[29] S. Baker, J. S. Robinson, C. A. Haworth, H. Teng, R. A. Smith, C. C. Chirilă, M. Lein, J. W. G. Tisch, and J. P. Marangos, Science **312**, 424 (2006).
[30] E. Goll, G. Wunner, and A. Saenz, Phys. Rev. Lett. **97**, 103003 (2006).
[31] T. Ergler, B. Feuerstein, A. Rudenko, K. Zrost, C. D. Schröter, R. Moshammer, and J. Ullrich, Phys. Rev. Lett. **97**, 103004 (2006).
[32] S. Baker, J. S. Robinson, M. Lein, C. C. Chirilă, R. Torres, H. C. Bandulet, D. Comtois, J. C. Kieffer, D. M. Villeneuve, J. W. G. Tisch, et al., Phys. Rev. Lett. **101**, 053901 (2008).
[33] L. Fang and G. N. Gibson, Phys. Rev. Lett. **100**, 103003 (2008).
[34] A. Saenz, J. Phys. B: At. Mol. Phys. **33**, 4365 (2000).
[35] A. Saenz, Phys. Rev. A **61**, 051402(R) (2000).
[36] A. Saenz, J. Phys. B: At. Mol. Phys. **33**, 3519 (2000).
[37] A. Saenz, Phys. Rev. A **66**, 063407 (2002).
[38] A. Saenz, Phys. Rev. A **66**, 063408 (2002).
[39] M. Awasthi and A. Saenz, J. Phys. B: At. Mol. Phys. **39**, S 389 (2006).
[40] X. Urbain, B. Fabre, E. M. Staicu-Casagrande, N. de Ruette, V. M. Andrianarijaona, J. Jureta, J. H. Posthumus, A. Saenz, E. Baldit, and C. Cornaggia, Phys. Rev. Lett. **92**, 163004 (2004).
[41] Y. V. Vanne and A. Saenz, J. Phys. B: At. Mol. Phys. **37**, 4101 (2004).
[42] L. Wolniewicz, J. Chem. Phys. **99**, 1851 (1993).
[43] L. Wolniewicz and K. Dressler, J. Chem. Phys. **100**, 444 (1994).
[44] K. Dressler and L. Wolniewicz, Ber. Bunsenges. Phys. Chem. **99**, 246 (1995).
[45] G. Staszewska and L. Wolniewicz, J. Mol. Spectrosc. **212**, 208 (2002).
[46] L. Wolniewicz and G. Staszewska, J. Mol. Spectrosc. **220**, 45 (2003).
[47] A. Lühr, Y. V. Vanne, and A. Saenz, Phys. Rev. A **78**, 042510 (2008).
[48] A. Lühr and A. Saenz, Phys. Rev. A **78**, 032708 (2008).
[49] A. Lühr and A. Saenz, Phys. Rev. A **79**, 042901 (2009).